Spontaneous formation of dual stratification patterns in a large quasi-two-dimensional sand pile

Michiko Shimokawa* and Shonosuke Ohta
Department of Earth System Science and Technology, Kyushu University, Kasuga, Fukuoka 816-8580, Japan
(Received 20 September 2007; published 18 January 2008)

By pouring a mixture of two types of grains into a large vertical cell with a narrow space, we discovered a dual stratification pattern consisting of two different wavelengths at the upper and lower regions of the resulting sand pile. In the formation of this pattern, we also observed an additional type of kink—a wave that moves toward the top of the sand pile along the slope. The kink, herein called a trapped kink, is essential for the formation of dual stratification patterns. Asymmetric probability distributions are obtained from measurement of the position where the kinks are generated. We proposed a phenomenological model to describe the kink generation process. The results analyzed by this model agree with experimental distributions.

DOI: 10.1103/PhysRevE.77.011305 PACS number(s): 45.70.Mg, 45.70.Qj, 45.70.Vn

I. INTRODUCTION

Interesting patterns, such as the formation of a band of regular stripes, a chaotic-regular structure, a petal pattern, and a stratification pattern, are formed spontaneously [1–6] when mixed grains are rotated in a cylinder [1–3] or a drum [4,5] and poured into a narrow space [6]. The formation of the above patterns is derived from the size segregation of mixed grains in an avalanche. Size segregation is an undesirable consequence for industrial processes, which require that mixed grains poured from a hopper remain homogeneous. The physical property of size segregation, however, is not yet fully understood, and its study is one of the developing topics in physics.

Patterns formed by pouring binary mixtures of grains into a narrow space are recognized as interesting examples of size segregation. When a binary mixture is poured into a narrow vertical cell, we observe either a segregation or a stratification pattern [6–10,12–14]. A segregation pattern occurs if the mixture consists of large smooth grains and small rough grains. In contrast, a stratification pattern occurs if the mixture consists of large rough grains (LRGs) and small smooth grains (SSGs). For both segregation and stratification patterns, the angle of repose and the size of each grain determine the pattern [6–10,14]. In this study, we focus on stratification patterns. A stratification pattern has alternating LRG and SSG stripes. The process by which a single pair of stripes is formed is as follows [8–10]: (1) a size segregation occurs in the avalanche in which the upper and lower avalanche layers are LRGs and SSGs, respectively; (2) the avalanche stops with the formation of a kink, which is an uphill wave of congestion generated at the bottom of the pile that moves toward the top of the pile; and (3) the uphill motion of the kink forms a distinct pair of layers. This process repeats itself and a stratification pattern emerges. A kink is important for the formation of this pattern. Many scientists have investigated kink generation [8–10,14]. It is reported that the kink is generated only at the bottom of the pile, because the incline of a sand pile decreases near the bottom [10]. We are interested in the static regular pattern, as well as the periodic motion of an avalanche and a kink.

We discovered a dual stratification pattern with two periodic stripes as shown in Fig. 1(b) and a different type of kink by performing experiments with a large vertical cell. Surprisingly, this kink is generated on a sand pile slope with a nondecreasing incline.

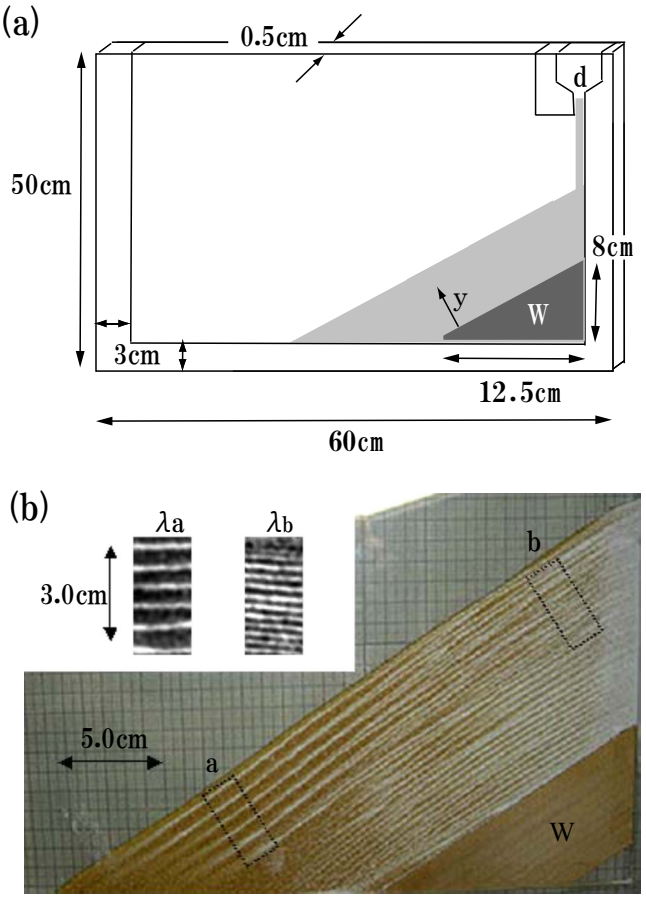

FIG. 1. (Color online) (a) Sketch of the experimental apparatus. The width of the funnel d varies, which leads to changes in the flux. The wooden board is shown as W. The distance from W is represented as y. (b) Dual stratification pattern with a large sand pile. Wavelengths in lower region a and upper region b of the sand pile are shown as λ_a=7.7 mm and λ_b=3.8 mm (flux 0.37 g/s), respectively.

*simokawa@esst.kyushu-u.ac.jp

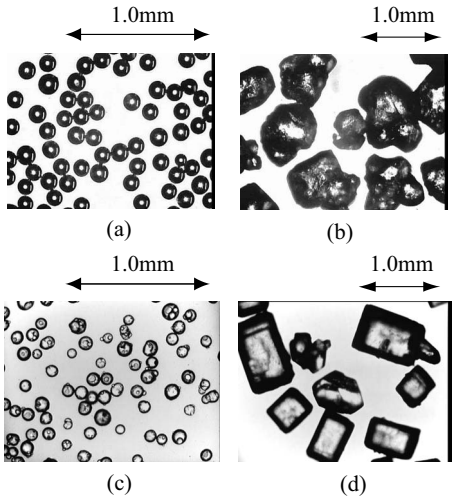

FIG. 2. Samples of (a) glass beads and (b) brown sugar. Tracers of (c) dry silica gel and (d) white sugar.

In this paper, we describe and report our findings on the self-organized dual stratification and, in particular, the developmental process of the kink. Preliminary results were reported in [11]. The remainder of this paper is organized as follows: Sec. II describes our experimental procedures; experimental results are presented in Sec. III; our proposed physical model is described in Sec. IV; and our conclusion is given in Sec. V.

II. EXPERIMENTAL PROCEDURES

We performed experiments using a vertical cell, as illustrated in Fig. 1(a). The vertical cell consists of two acrylic sheets, each with a thickness of 0.5 cm. The width of the vertical cell is 72.0 cm, and the vertical length is 56.0 cm. The size we selected is approximately twice the conventional size [6,7,9,12] used to study the details of a stratification pattern. The two acrylic sheets are mounted parallel to one another on a horizontal base plate. The space between the two parallel sheets is 0.5 cm. During the formation of a large sand pile, the foundation of the pile sometimes sinks and the pile collapses. Therefore, a triangular wooden board W was built to prevent the sand pile from collapsing. The wooden board W is 12.5 cm long and 8.0 cm high. The slope of W is 33°, which is equal to the repose angle of the sand pile in the stratification pattern. The upper layer of the stripe structure consists of LRGs; further, there are only LRGs on the surface of the sand pile. Therefore, to replicate a real sand pile, we pasted LRGs on the surface of W. If the vertical distance y from W is greater than 10 cm, we confirm that W does not influence the dual stratification. Therefore, we performed experiments at $y=12.5\pm2.5$ cm. The binary mixture consisted of tiny glass beads and brown sugar, corresponding to SSGs and LRGs, respectively, as shown in Figs. 2(a) and 2(b). The diameter of each glass bead was 0.1 mm, while the brown sugar grains ranged from 0.2 to 0.8 mm in diameter. The repose angles of the SSGs and LRGs were 27° and 38°, respectively. For our experiments, the two types of grains are uniformly mixed in the volume ratio of 1:1. Grains of dry silica gel and white sugar [refer to Figs. 2(c) and 2(d)] are used as tracers to investigate the granular movement under an avalanche. We added these tracers at a rate of 5% of the mixture grains. Their physical properties, including diameter and repose angle, are almost the same as those of the glass beads and brown sugar grains. In our experiment, the influence of mixing in the tracers is negligible. The granular mixture was poured through a funnel at the right edge of the vertical cell, as shown in Fig. 1(a). The flux J of the mixture is the total mass of grains poured per second, which depends on the width d of the funnel. We used a SONY DCR-VX2100 digital video camera to observe the dynamic behavior of the stratification pattern. The shutter speed was 1/60 s and the resolution was set to 640×480 pixels. The videos recorded with the camera were processed at intervals of 0.13 s. The experimental temperature was 20 ± 2 °C, and was performed at a room humidity of (41 ± 4)% since special care had to be taken to prevent cohesion due to moisture.

III. EXPERIMENTAL RESULTS

A. Dual stratification

Using a large-size vertical cell [as shown in Fig. 1(a)], we discovered the dual stratification pattern shown in Fig. 1(b). Although ordinary stratification is reported to have a single wavelength [12,13], the dual stratification pattern has two different wavelengths in the upper and lower regions of the sand pile. The wavelength λ_a in the lower region and the wavelength λ_b in the upper region were analyzed using power spectra obtained from the fast Fourier transform algorithm. For a flux $J=0.37$ g/s, λ_a and λ_b are 7.7 and 3.8 mm, respectively. A dual stratification with two different wavelengths at the upper and lower regions ($\lambda_a=2\lambda_b$) is observed in the present experiments using a large vertical cell.

B. Formation dynamics of dual stratification

A kink is observed in the emergence of the dual stratification pattern. In past experiments with a small sand pile, a kink was produced only at the bottom of the sand pile [6–10,12–14]. In general, the incline of a sand pile decreases near the bottom and the avalanche stops. As a result, a kink occurs only at the bottom. On the contrary, in our experiment with a larger sand pile, a kink is generated not only at the bottom, but also on the slope. We term this phenomenon a "trapped kink." The trapped kink is essential in the formation of the dual stratification pattern.

In our experiments, we investigated the generation of the trapped kink using a digital video camera. The aforementioned mixture was poured from the edge of the vertical cell and an avalanche formed. The binary mixture separates into two layers of LRGs and SSGs as it moves down the slope. According to the size segregation in an avalanche [14], the LRGs concentrate at the upper layer of an avalanche, and the SSGs at a lower layer. We call this region "two-layer flow."

The LRGs in the upper layer are faster than the SSGs in the lower layer; therefore, LRGs gather at the head of the avalanche. We call this area, which is made up of only LRGs, the "LRG head." The LRG head accumulates with

time. When a sufficient amount of LRGs gather at the head, the LRG head stops growing and is solidified on the sand pile slope. This solidified LRG head acts as a barrier and blocks the movement of the two-layer flow. The two-layer flow continues to collide with the solidified avalanche and itself solidifies toward the top.

By the process described above, a trapped kink is formed. A stripe of LRGs and SSGs is formed between the top of the sand pile and the position where the trapped kink is generated. After the trapped kink arrives at the top, the next avalanche occurs. Since the head of a solidified avalanche is too steep, the next avalanche cannot stop on the slope and therefore stops at the bottom. Therefore, a normal kink is generated at the bottom and traverses upward. Meanwhile, a stripe is formed going toward the top from the bottom of the sand pile. After this normal kink passes up the slope, the surface of the slope becomes nearly flat. The avalanche that occurs after the normal kink can stop on the sand pile slope with a its flat surface, and a trapped kink is generated again. The above processes are repeated.

The frequency of kink generation in the upper region is approximately twice that in the lower region. The uphill motion of a kink forms a pair of stripes with alternating LRGs and SSGs. The lower wavelength λ_a is produced only by the normal kink, while the upper wavelength λ_b is produced by the normal kink and the trapped kink. Therefore, λ_a is approximately twice λ_b. The fairly constant repetition of the trapped kink and the normal kink creates this dual stratification pattern.

C. Asymmetric distribution of trapped kink generation

The trapped kink generation is important for the formation of dual stratification. The position ℓ at which a trapped kink is generated varies; it is not constant as shown in the observations of trapped kinks in Fig. 3(a). In this section, we investigate the probability distribution $f(\ell)$ of ℓ. Our aim is to understand the trapped kink generation. By comparing $f(\ell)$ obtained from experiments in this section and proposed models in Sec. IV, we will understand the trapped kink generation.

The position ℓ is measured parallel to the sand pile slope, and is defined as 0 at the top of the sand pile. The definition of $f(\ell)$ is

$$f(\ell) = \frac{n_l}{N\,\Delta\ell}, \tag{1}$$

where n_l is the number of trapped kinks generated in a range from $\ell - \Delta\ell/2$ to $\ell + \Delta\ell/2$, N is the total number of samples $N = \Sigma_\ell n_\ell$, and $\Delta\ell$ is the step size. A transparent sheet is pasted in the surface of the vertical cell. In the observation of the trapped kink, points mark the positions ℓ on the sheet. Afterward, $f(\ell)$ is determined by counting the points recorded on the sheet. In our experiments, $N \approx 250$ and $\Delta\ell = 1.18$ cm.

The data shown in Fig. 3(a) were measured with $J = 0.86$ g/s. As seen in this figure, the characteristic feature of the obtained distribution $f(\ell)$ is its asymmetric profile. In general, symmetric distributions such as Gaussians are derived from merely random white noise; whereas, surprisingly, our distribution has nontrivial asymmetry. In this section, we focus on the asymmetric profiles of $f(\ell)$.

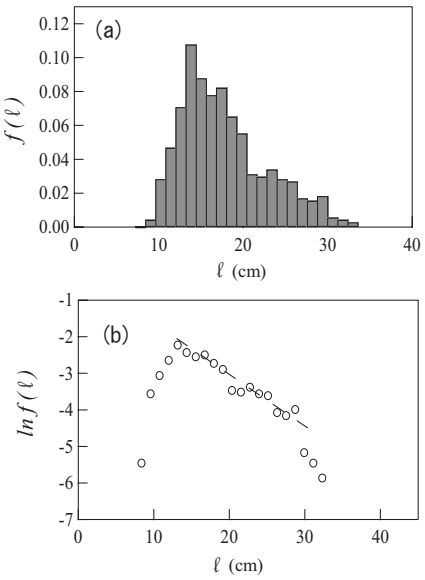

FIG. 3. Distribution $f(\ell)$ of position ℓ where a trapped kink is generated. The vertical axis of (a) is a linear scale, while that of (b) is logarithmic. Data at tail region can be fitted with the exponential $\exp(-\gamma\ell)$, where $\gamma = 0.17$ (flux 0.86 g/s).

The behavior at $\ell > \ell_0$ is different from that at $\ell < \ell_0$, where ℓ_0 is the peak position of the distribution. At $\ell > \ell_0$ the exponential function shown in Fig. 3(b) is the best-fitting function, rather than a log-normal or logarithmic distribution. Therefore, we assume

$$f(\ell) \sim \exp(-\gamma\ell), \tag{2}$$

where the coefficient γ is 0.17 for flux $J = 0.86$ g/s. The Gaussian distribution is found to be the best-fitting function for $f(\ell)$ at $\ell < \ell_0$.

It is important from a physical point of view to understand the origins of these Gaussian and exponential functions. In what follows, $f(\ell)$ at various fluxes and vertical distances from a wooden board is investigated. These results give us good suggestions about the dynamical mechanism of trapped kink generation.

1. Flux dependence

In this section, we focus on the distribution $f(\ell)$ at various fluxes. We measured data points at $y = 12.5 \pm 2.5$ cm. Figure 4(a) shows $f(\ell)$ for $J = 0.19$, 0.59, and 1.15 g/s. These distributions have two common features. First, the peak position ℓ_0 increases with J. As shown in Fig. 4(b), ℓ_0 increases in proportion to J. Second, all distributions are asymmetric for all J. Let $f_J(\ell)$ be the distribution at flux J. To evaluate these asymmetric profiles qualitatively, we consider the following transformation:

$$\tilde{f}_J(\ell) = a(J) f_J(\ell'), \tag{3}$$

where $a(J) = f_s(\ell_0(J_s))/f_J(\ell_0(J))$ is a scaling parameter, and $\ell' = a(J)[\ell - \ell_0(J_s)] + \ell_0(J)$. After the transformation, we rec-

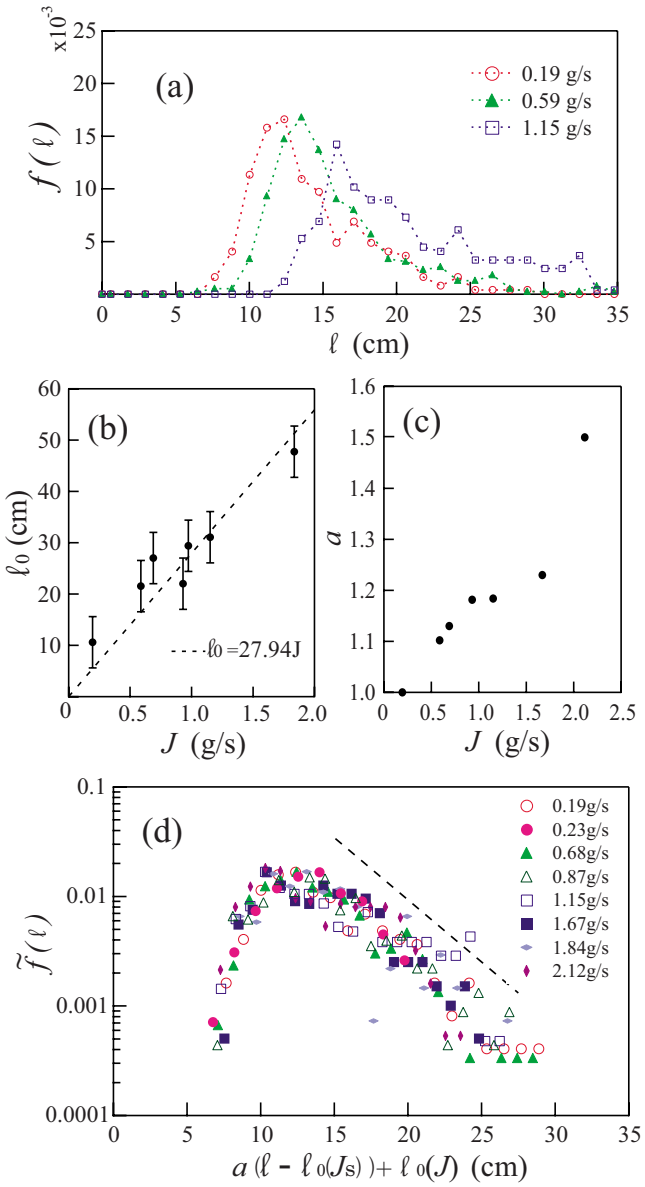

FIG. 4. (Color online) (a) Flux dependence of distribution $f(\ell)$. Data for flux $J=0.19$, 0.59, and 1.15 g/s are shown as open circles, closed triangles, and open squares, respectively. (b) Flux dependence of peak position ℓ_0. (c) Flux dependence of transformation parameter a. (d) Transformed results $\tilde{f}(\ell)$ for each flux distribution $f(\ell)$.

ognize the distribution $f_s(\ell)$ at $J_s=0.20$ g/s as the standard distribution $[\tilde{f}_s(\ell)=f_s(\ell)]$.

We derive the transformation as follows: (1) the distribution $f_J(\ell)$ is horizontally shifted by $-\ell_0(J)$ so that it has its peak at the origin; (2) the shifted distribution is expanded (shrunk) vertically by multiplying it by $a(J)$ such that we have the same peak value as in the distribution with $J_s=0.19$ g/s; (3) the distribution is shrunk (expanded) horizontally for normalization; and (4) the distribution is shifted again so that it has its peak at $\ell=\ell_0(J_s)$.

These processes are applied to all distributions. Figure 4(c) shows the flux dependence $a(J)$ used in the above transformation; $a(J)$ increases with the flux. Figure 4(d) shows the results of the above transformations. All distributions are asymmetric, which agrees with $f_s(\ell)$ in Fig. 4(d). In particular, these distributions are almost exponential for $\ell > \ell_0(J_s)$. This confirms that all distribution functions are common for a variety of fluxes.

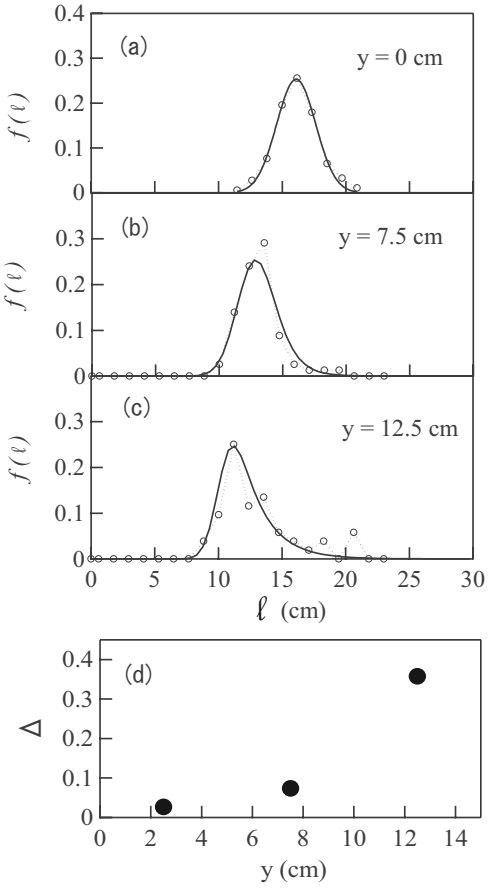

FIG. 5. Distribution $f(\ell)$ at vertical distance y from wooden board. Open circles are experimental data and solid line shows fitting, which is Gaussian in (a) and drawn using Eq. (11) in (b) and (c). $y=$(a)0, (b) 7.5 ± 2.5, and (c) 12.5 ± 2.5 cm. (d) Degree of asymmetry Δ of distribution $f(\ell)$ at $y=2.5\pm2.5$, 7.5 ± 2.5, and 12.5 ± 2.5 cm, where y is the vertical distance from the wooden board (flux 0.10 g/s).

2. Dependence on vertical distance from wooden board

In this section, we investigate the distribution $f(\ell)$ for various values of y, where y is the vertical position from the wooden board W shown in Fig. 1(a). The value of y is defined as 0 at the surface of W. The flux is 0.10 g/s. Figures 5(a)–5(c), show $f(J)$ at $y=0$, 7.5 ± 2.5, and 12.5 ± 2.5 cm, respectively.

As shown in the figures, ℓ_0 decreases as y increases. To understand this phenomenon, consider the following scenario. Let H be the drop length of grains poured from a funnel. The relation between H and y is $H=H_0-y/\cos\theta_{st}$, where H_0 is the length with $y=0$ and θ_{st} is the repose angle of the sand pile. If H is large, the potential energy of the grains is also large. Since the potential energy decreases with

increasing y, ℓ_0 also tends to decrease with increasing y.

To be specific, $\ell_0 = -0.35y + 15.64$ at 0.10 g/s. We calculate $f(\ell)$ for $y=0$, 2.5 ± 2.5, 7.5 ± 2.5, and 12.5 ± 2.5 cm under the same conditions (i.e., the same H). Although the resulting profiles are different, each ℓ_0 is the same, thus confirming that differences of ℓ_0 are nonessential for trapped kink generation.

Next, we focus on the profiles of $f(\ell)$ with various values of y. $f(\ell)$ at $y=0$ is best fitted with a Gaussian distribution, which is depicted as a solid line in Fig. 5(a). This result indicates that random white noise causes the distribution at $y=0$; whereas asymmetric distributions are obtained at $y > 0$, as shown in Figs. 5(b) and 5(c). In order to evaluate the asymmetry quantitatively, we define and calculate the degree of asymmetry of the distribution $\Delta(y)$ at 2.5, 7.5, and 12.5 cm as

$$\Delta = \int_0^{+\infty} [f(\ell) - G(\ell)] d\ell, \tag{4}$$

where the Gaussian distribution $G(\ell)$ is decided by fitting the data at $\ell < \ell_0 + \Delta\ell$. In Fig. 5(d), $\Delta(y)$ increases with y for $J = 0.10$ g/s.

The above results show that y has a great influence on the distribution profile. It is considered that $\Delta(y)$ indicates degree of the interaction between an avalanche and the grains underneath, and the degree increases with y. This means that the distribution profiles depend on the ground condition, which forms the foundation for the physical models in Sec. IV.

IV. PHYSICAL MODEL

In this section, we consider a phenomenological model for trapped kink generation. Our trapped kink model, introduced in Sec. IV A, predicts the position ℓ where the trapped kink is generated. The model tends to agree with the experimental peak position ℓ_0; however, the model does not offer a satisfactory account of the dynamics of trapped kink generation.

One of the reasons our model is lacking in this regard is that it does not consider the interaction between an avalanche and the grains underneath, which is important, based on results of Sec. III C. Therefore, we propose an improved model in Sec. IV B, in which the interaction is considered. The results show the same features as the experimental distributions for $\ell > \ell_0$ [as given in Fig. 3(b)].

Combining the two models mentioned above, we describe a hybrid model in Sec. IV C. The distribution defined by this model agrees with the experimental distribution.

A. Trapped kink model

Figure 6 shows images of the LRG head. The lower drawings are schemata of the images shown above. Figure 6(a) represents data at $x(t) < \ell$ before trapped kink generation, where $x(t)$ and ℓ are the positions at the head of an avalanche and at the onset of trapped kink generation, respectively. The LRG head descends as an avalanche. Figure 6(b) is a photograph in which $x(t) = \ell$ after a trapped kink is generated. At that moment, the LRG head does not move and is stationary. Comparing Figs. 6(a) and 6(b), the head angle $\theta(t)$ decreases as time increases. From the geometric relationship shown in Fig. 6, we find

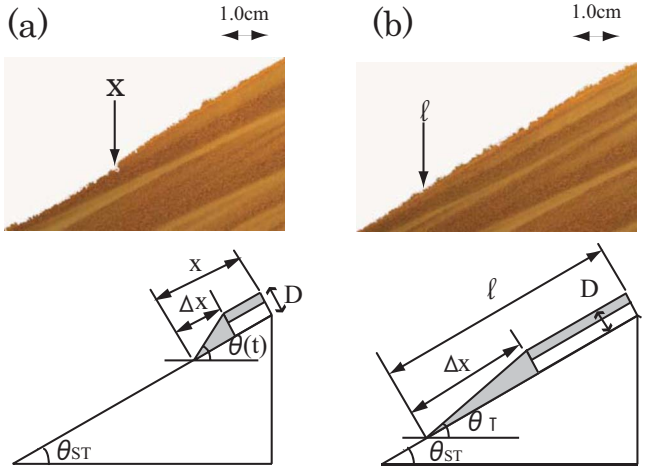

FIG. 6. (Color online) Snapshots of LRG head (a) when the avalanche descends onto the sand pile slope and (b) when the trapped kink is generated. Length of avalanche and LRG head are shown as x and Δx, respectively. The position where the trapped kink is generated is shown as ℓ. Angles for the sand pile and head of the avalanche are shown as θ_{ST} and $\theta(t)$, respectively. Thickness of avalanche is D (flux 1.64 g/s).

$$\theta(t) = \theta_{ST} + \arctan\left(\frac{D}{\Delta x}\right), \tag{5}$$

where θ_{ST}, D, and Δx represent the repose angle of the sand pile, the thickness of the two-layer flow, and the length of the LRG head, respectively.

The following results were obtained from Ref. [13]: (1) D is approximately constant in an avalanche; and (2) $\Delta x(t)$ increases in proportion to $x(t)$. These data are measured as follows. (1) We track an avalanche with the digital video camera until a trapped kink is generated. (2) The obtained movie data are transformed to photographs approximately every 0.33 s by Windows Movie Maker. (3) By comparing two successive photographs, the results, such as constant D and the relation between $\Delta x(t)$ and $x(t)$, are investigated.

Equation (5) shows that an increase of $\Delta x(t)$ causes a decrease of $\theta(t)$. We measure $\theta(t) = \theta_T$ when a trapped kink is generated by using snapshots as shown in Fig. 6(b). The angle θ_T is $(38.4 \pm 1.4)°$, which agrees with the repose angle of the LRGs, θ_{LR}. We conjecture that a trapped kink is generated when $\theta(t) = \theta_{LR}$. We name this conjecture the trapped kink (TK) model. By applying the TK model and a substitution of $\Delta x = \alpha x$ and $\theta(t) = \theta_{LR}$ in Eq. (5), we obtain

$$\ell = \frac{D}{\alpha \tan(\theta_{LR} - \theta_{ST})}. \tag{6}$$

For a flux of 0.86 g/s, $D=0.7$ cm, $\theta_T - \theta_{ST} = \theta_{LR} - \theta_{ST} = 5.4°$, and $\alpha = 0.63$. Inserting these values into Eq. (6), we obtain $\ell = L_T = 11.8 \pm 2.6$ cm. Therefore, the TK model results

closely agree with the peak position $\ell_0=13.2$ cm (obtained from experiments as shown in Fig. 8).

Let us also consider the phenomena at $\theta(t)=\theta_{LR}$. The idea of the TK model is based on the formation process of a sand pile. The phenomena occurring at the repose angle of θ_{LR} on the pile are often compared to a phase transition. For slopes in which $\theta(t)\leqslant\theta_{LR}$, no flow of sand can occur and the pile appears to be a solid; whereas for $\theta(t)>\theta_{LR}$, the surface layers of the pile freely flow on the slope as a liquid. In other words, the liquid pile at the surface transforms to a solid state when $\theta(t)=\theta_{LR}$.

According to the above demonstration, we focus on the states of the LRG head. At first, for $\theta(t)>\theta_{LR}$, the LRG head cannot stop and descends as an avalanche (like a liquid). Later, for $\theta(t)=\theta_{LR}$, the LRG head changes from a liquid to a solid state. In our experiments with a large sand pile, the slope length is larger than that of previous experiments. Due to the long slope, a large number of LRGs gather at the head of the avalanche, which results in $\theta(t)=\theta_{LR}$ and a solidified LRG head.

B. Survival probability model

The TK model agrees with ℓ_0, showing a Gaussian distribution. The behavior at $y=0$, where $f(\ell)$ is almost fitted with a Gaussian distribution [as shown in Fig. 5(a)], is explained by the TK model. The degree of asymmetry Δ of $f(\ell)$, however, increases with y as shown in Fig. 5(d), which is not explained by the TK model. Therefore, we need to consider improved models.

A characteristic feature at $y>0$ is that the region at $\ell>\ell_0$ follows an exponential distribution [see Fig. 3(b)]. Let us focus on the exponential decay. The exponential decay is explained by using a probability model. We consider a distribution with sample number N. By assuming that an avalanche stops with probability A per unit length, the number of avalanches that stop at length ℓ are

$$NA(1-A)^{\ell-1}=\frac{1}{1/A-1}N(1-A)^{\ell}=\mu q^{\ell}. \tag{7}$$

where $\mu=N/(1/A-1)$ and $q=1-A$. The value of μq^{ℓ} corresponds to $f(\ell)$. Equation (7) shows the exponential decay of $f(\ell)$ for $\ell>\ell_0$. The dominant factor is q, which plays a key role in trapped kink generation. The physical parameter $q=1-A$ is the probability that an avalanche continues to descend. If we consider the stopping of the avalanche and the generation of a trapped kink as the death of an avalanche, q means the survival probability of the avalanches.

The flux dependence of q is shown in Fig. 7(b), which is obtained from experiments. This figure shows that q increases with J and the fitting function is $q=0.25J+0.65$.

From results of Fig. 5, it is considered that the interaction between an avalanche and the grains underneath has a great influence on q. The interaction causes granular movements under an avalanche, which is termed transient creeplike motion. In general, a creep motion shows the underlying granular movement in the flow of an avalanche [15] as shown in Fig. 7(a). The transient creeplike motion is derived from the force applied when an avalanche begins to stop, and is observed until the avalanche stops.

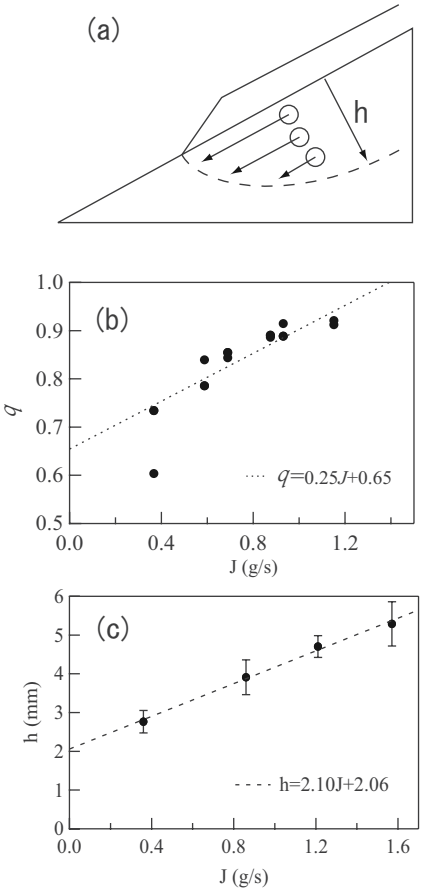

FIG. 7. (a) Sketch of transient creeplike motion, where h is the vertical distance of the motion. (b) Flux dependence of survival probability q. (c) Flux dependence of vertical depth h. Closed circles and dotted lines in (b) and (c) show experimental data and fitting lines, respectively.

Focusing on the creeplike motion before and after a trapped kink is generated, the depth h in Fig. 7(a), which is the region of this motion, is measured. The surface of the slope is defined as $h=0$. We compare the image at 1 s before a trapped kink is generated to the image at 1 s after generation. The granular mixtures include dry silica gel and white sugar as tracers. The value of h is obtained from measurements of the tracer positions before and after trapped kink generation. Figure 7(c) shows that h increases according to $h=2.10J+2.06$. The results of $q=0.25J+0.65$ and the above relation between h and J yield $q=0.12h+0.4$.

Given the linear relation of q and h, the transient creeplike motion has a great influence on the survival probability q. The creeplike motion causes the solidified avalanche, which is shown in the TK model, to be unable to stop. For large h, the ground will be unstable due to the creeplike motion, and grains under an avalanche will be easy to move and will slide around, which corresponds to a large q. The survival probability (SP) model shows the effect of the transient creeplike motion on trapped kink generation.

C. Model for an asymmetric distribution

Combining the TK and SP models introduced in Secs. IV A and IV B, respectively, our combined model clarifies trapped kink generation and provides an asymmetric distribution. In this section, we describe the formation of the hybrid model along with results that agree with the experimental data.

If there is no transient creeplike motion, a trapped kink is generated when $\theta(t)=\theta_{LR}$; however, according to the TK model, an avalanche cannot stop at $\theta(t)=\theta_{LR}$ if the creeplike motion occurs. Trapped kink generation occurs as follows: (1) when $\theta(t)=\theta_{LR}$, the LRG head is solidified; and (2) the solidified LRG head stops when the creeplike motion disappears.

First, consider step 1 mentioned above. The distribution obtained from the TK model is Gaussian, yielding

$$t(\ell') = \frac{1}{\sqrt{2\pi\sigma^2}} \exp\left(-\frac{(\ell'-L_T)^2}{2\sigma^2}\right), \tag{8}$$

where σ is the variance and L_T is the value obtained from the TK model. As mentioned earlier, the distribution at $y=0$ almost fits a Gaussian distribution, where trapped kink generation is described by only the TK model because there is no creeplike motion at $y=0$.

We cannot disregard transient creeplike motion when $y>0$. Next, we consider step 2 as $s(\ell)$, which represents the transient creeplike motion under an avalanche. When $\theta(t)=\theta_{LR}$ at ℓ' and an avalanche stops at ℓ $(\ell>\ell')$,

$$s(\ell) = \gamma \exp[-\gamma(\ell-\ell')], \tag{9}$$

where $\exp(-\gamma)$ corresponds to the survival probability q. Equation (9) is based on the SP model.

The probability density distribution $F(\ell)$, which is a combination of $t(\ell')$ and $s(\ell)$, is

$$\begin{aligned} F(\ell) &= \int_0^{+\infty} d\ell'\, \theta(\ell-\ell') t(\ell') s(\ell) \\ &= \frac{\gamma}{\sqrt{2\pi\sigma^2}} \int_0^{+\infty} d\ell'\, \theta(\ell-\ell') \\ &\quad \times \exp\left(-\frac{(\ell'-L_T)^2}{2\sigma^2}\right) \exp[-\gamma(\ell-\ell')], \end{aligned} \tag{10}$$

where $\theta(\ell-\ell')=0$ at $\ell<\ell'$ and $\theta(\ell-\ell')=1$ at $\ell>\ell'$.

To confirm our conjecture, we compare the experimental distribution $f(\ell)$ with the model distribution $F(\ell)$. Using Eq. (10), the discrete equation

$$\begin{aligned} F(m) &= \frac{1-\exp(-\gamma a)}{\sqrt{2\pi\sigma^2}} \sum_{n=0}^{+\infty} \theta(m-n) \\ &\quad \times \exp\left(-\frac{(na-L_T)^2}{2\sigma^2}\right) \exp[-\gamma(m-n)a] \end{aligned} \tag{11}$$

is obtained, where a is the step size, $ma=\ell$, and $na=\ell'$. Equations (10) and (11) contain both the Gaussian term $t(\ell')$ and the exponential term $s(\ell)$, and $s(\ell)$ plays a role as a correction function for $t(\ell')$.

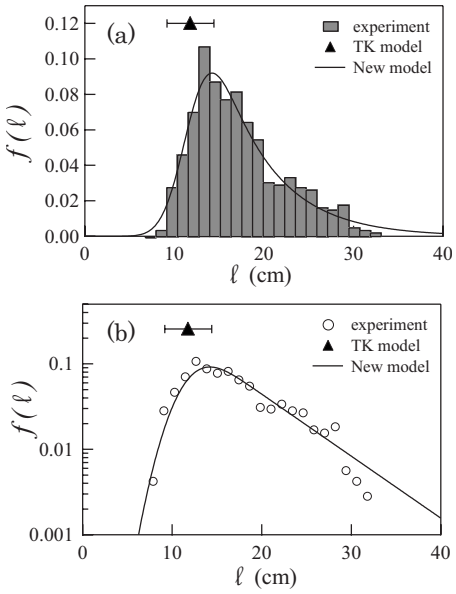

FIG. 8. Distribution $f(\ell)$ of position ℓ where trapped kink is generated. Result of TK model is shown as filled triangle, 11.8 ± 2.6 cm. Peak value of distribution obtained from experimental result is 13.2 ± 0.5 cm, which is almost the same as the result of the TK model. The solid line is the fitting line by our hybrid model. The parameters of this model are $\sigma=2.40$, $\gamma=0.17$, and $L_T=11.8$. The line agrees with experimental data. The vertical axes of (a) and (b) are linear and logarithmic, respectively (flux=0.86 g/s).

The number of solidified LRGs is small at $\ell<\ell_0$, where it is essential that the LRG head is solidified. Therefore, $F(\ell)$ at $\ell<\ell_0$ almost follows a Gaussian distribution, as seen in Fig. 8(a). When $\ell>\ell_0$, most of the LRG head is solidified and the transient creeplike motion becomes essential for trapped kink generation. Therefore, as shown in Fig. 8(b), $F(\ell)$ at $\ell>\ell_0$ decreases according to an exponential distribution. In response to these results, the variance σ is determined by fitting $f(\ell)$ at $\ell<\ell_0+\Delta\ell$ with $t(\ell')$; likewise, γ is determined by fitting $s(\ell)$ at $\ell>\ell_0$. Therefore, $\sigma=2.40$, $L_T=11.80$, and $\gamma=0.17$ for $f(\ell)$ at $J=0.86$ g/s and $y=12.5\pm2.5$ cm. The fitting curve $F(\ell)$, which is obtained by substituting the above parameters, is shown as a solid line in Fig. 8. As shown in Fig. 8(a), $F(\ell)$ agrees with the experimental distribution $f(\ell)$.

Returning to Fig. 5, recall that the solid lines in the figure represent Eq. (11), which agrees with experimental data. Parameters for Eq. (11) are shown in Table I. The distribution when $y=0$ fits a Gaussian distribution, which is obtained by determining $\lim_{\gamma\to+\infty}F(\ell)$. The limit is derived from $\lim_{\gamma\to+\infty}q=\lim_{\gamma\to+\infty}[\exp(-\gamma)]\sim0$, which means the survival

TABLE I. Parameters of Eq. (11) with various y.

y (cm)	L_T (cm)	σ	γ
0	16.41	2.05	$+\infty$
7.5	13.02	1.29	0.9
12.5	11.14	0.93	0.5

probability q does not exist. In fact, when $y=0$, there is no creeplike motion essential for q.

We have observed that $q=\exp(-\gamma)$ increases with y. For large y, the grains under an avalanche easily collapse and slide. Therefore, an avalanche finds difficulty stopping when $\theta(t)=\theta_{LR}$, indicating the increase of q with y. Our model of Eq. (10) is therefore natural.

A variety of distributions obtained from experiments fit our hybrid model, indicating that the following are essential for trapped kink generation: (1) an avalanche is solidified in $\theta(t)=\theta_{LR}$; and (2) the transient creeplike motion disappears.

V. CONCLUSIONS

From this study, we have discovered a dual stratification pattern, as shown in Fig. 1(b), for which we have performed experiments using a large vertical cell. The size of the vertical cell is approximately twice that of previous experiments [6,8,9,14], forging new ground in our field of study. The dual stratification pattern has two different wavelengths at the upper and lower regions of the sand pile ($\lambda_a=2.0\lambda_b$).

We have also observed a "trapped kink" during the formation of dual stratification patterns. The trapped kink is generated on the sand pile slope, which in turn is essential for the formation of a dual stratification pattern.

Asymmetric probability density distributions are obtained from measurements of the position ℓ at which the trapped kink is generated. The typical feature is the exponential decay $\exp(-\gamma\ell)$ at $\ell>\ell_0$, where ℓ_0 is the peak position of the distribution (refer to Fig. 3). The distribution profiles depend on distance y from the wooden board W [see Figs. 5(a)–5(c)], although the asymmetric profiles remain at a variety of fluxes (see Fig. 4). The degree Δ of asymmetry becomes large with increasing y [see Fig. 5(d)]. In particular, at $y=0$, the distribution almost follows a Gaussian distribution.

We consider two phenomenological models. One is the trapped kink model, and the other is the survival probability model.

The value of 11.8 ± 2.6 cm obtained from the trapped kink model agrees with the experimental value $\ell_0=13.2$ cm within experimental error (for $J=0.86$ g/s). This model assumes that an avalanche is solidified when $\theta(t)=\theta_{LR}$.

The survival probability model incorporates exponential decay for $\ell>\ell_0$. The key factor $q=\exp(-\gamma)$ describes the probability that an avalanche continues to descend. For $J=0.86$ g/s, $\gamma=0.17$ is obtained through experimentation. Figure 7 shows $q\propto J$ and $h\propto J$. These results imply $q\propto h$, which further implies that transient creeplike motion for grains under an avalanche has an impact on the exponential decay.

Our proposed hybrid model, which is a combination of the TK and SP models, as shown in Fig. 8, produces results that agree with experimental distributions. Through our hybrid model, we propose a distribution function formed from both Gaussian and exponential distributions.

In nature, numerous phenomena show asymmetric distributions; however, it is difficult to completely understand these phenomena. One cause of this difficulty is that each interaction is too large to properly consider. In our experiments, the interactions are collisions of each grain under an avalanche and collisions between an avalanche and the grains underneath. Using our hybrid model, some asymmetric distributions may be fitted, and lead to a better understanding of complex physical properties in nature.

ACKNOWLEDGMENTS

We would like to thank H. Honjo, S. Sakaguchi, H. Katuragi, H. Nakanishi, N. Mitarai, and M. Isobe for their helpful suggestions, discussions, and comments; R. Baba for his helpful programming; A. Nakahara for introducing pattern formation in physics; and M. Homma for reviewing our manuscript and helpful good suggestions. Our research was sponsored by the Japan Society for the Promotion of Science for Young Scientists.

[1] O. Zik, D. Levine, S. G. Lipson, S. Shtrikman, and J. Stavans, Phys. Rev. Lett. **73**, 644 (1994).
[2] K. M. Hill, A. Caprihan, and J. Kakalios, Phys. Rev. Lett. **78**, 50 (1997).
[3] K. M. Hill, Nitin Jain, and J. M. Ottino, Phys. Rev. E **64**, 011302 (2001).
[4] Hernan A. Makse, Phys. Rev. Lett. **83**, 3186 (1999).
[5] I. Zuriguel, J. M. N. T. Gray, J. Peixinho, and T. Mullin, Phys. Rev. E **73**, 061302 (2006).
[6] H. A. Makse, S. Havlin, P. R. King, and H. E. Stanley, Nature (London) **386**, 379 (1997).
[7] Y. Grasselli and H. J. Herrmann, Granular Matter **1**, 43 (1998).
[8] H. A. Makse, P. Cizeau, and H. E. Stanley, Phys. Rev. Lett. **78**, 3298 (1997).
[9] H. A. Makse, R. C. Ball, H. E. Stanley, and S. Warr, Phys. Rev. E **58**, 3357 (1998).
[10] J. M. N. T. Gray and Y. C. Tai, in *Physics of Dry Granular Media*, edited by H. J. Herrmann, J. P. Hovi, and S. Luding (Kluwer Academic Publishers, Boston, 1997), p. 697.
[11] M. Shimokawa and S. Ohta, Phys. Lett. A **366**, 591 (2007).
[12] J. P. Koeppe, M. Enz, and J. Kakalios, Phys. Rev. E **58**, R4104 (1998).
[13] H. A. Makse and H. J. Herrmann, Europhys. Lett. **43**, 1 (1998).
[14] Pierre Cizeau, Hernan A. Makse, and H. E. Stanley, Phys. Rev. E **59**, 4408 (1999).
[15] T. S. Komatsu, S. Inagaki, N. Nakagawa, and S. Nasuno, Phys. Rev. Lett. **86**, 1757 (2001).